Finite element analysis of second order wave resonance by multiple cylinders in a uniform current

Y.F. Yang[a, b], C.Z. Wang[a, *]

[a]*Ocean College, Zhejiang University, Zhoushan, 316021, China*

[b]*Department of Mechanical Engineering, University College London, Torrington Place, London WC1E 7JE, UK*

Abstract

The purpose of this paper is to study the diffraction of second order Stokes waves by four cylinders in a uniform current and mainly focus on the near-trapping phenomenon. A time domain second-order theory is employed to establish the mathematical model by splitting the total potential into the disturbed velocity potential caused by current, the first- or linear and second-order potentials, which satisfy their own boundary conditions. Each potential is calculated through the finite element method (FEM). Numerical results for four bottom-mounted cylinders in a uniform current are provided to show the resonant behaviour of waves and hydrodynamic forces including linear and second order at near-trapped frequencies, and the current effect on the wave and force are also analysed and discussed. Some results for a single- and four-cylinder cases are compared with previous studies.

Keywords: second order wave diffraction, finite element method, wave resonance, uniform current, multiple cylinders

1. Introduction

The interaction between waves and multiple structures such as oil platform and maritime bridge has been extensively investigated in offshore engineering. For example, linear wave radiation and diffraction by a group of cylinders were studied by Williams and Demirbilek [1], Williams and Abul-Azm [2], Butler and Thomas [3], Williams and Li [4], Walker and Taylor [5] and Siddorn and Taylor [6], and second order nonlinear problems were investigated by Abul-Azm and Williams [7, 8], Williams et al. [9] and Ghalayini and Williams [10]. One of the most interesting topics in the field of interactions between wave and multiple structures is the wave resonance at near-trapped frequencies. The finite wave energy mainly distributes within the region between multiple structures rather than propagating into infinity when the trapped mode happens, which is first described by Ursell [11]. Investigation on the trapped mode phenomenon is beneficial to prediction of the maximum wave run-up and hydrodynamic force, which is of vital importance for the design guidance of ocean structures. Linear wave diffraction by long array of cylinders up to 101 was studied by Maniar and

* Corresponding author. E-mail: cz_wang@zju.edu.cn

Newman [12] and small one such as four cylinders by Evans and Porter [13] at trapped modes in the frequency domain. Malenica et al. [14] further investigated second order near-trapped modes for four-cylinder cases. Wang and Wu [15] simulated the first- and second- order near-trapping phenomenon of the four-cylinder case and the Neumann trapped mode of a longer array of ten cylinders by time domain method. All these studies indicated that the wave elevation at some positions will significantly increase at the near-trapped frequencies. The near-trapping phenomenon of multiple elliptical cylinders in waves was also investigated by Chen and Lee [16] and Chatjigeorgiou and Katsardi [17]. In addition to theoretical and numerical research, some experimental studies were carried out by Kagemoto et al. [18]. Other investigations on multiple structures include those by Walker and Taylor [5], Walker et al. [19], Grice et al. [20] and Bai et al. [21]. However, none of these studies considered the effect of current.

To the best of our knowledge, little work on interactions between waves and multiple structures considered the current effect. However, the current usually coexists with the wave. A lot of works on wave-current-structure interaction may be found and they are mainly about a single isolated body such as linear problems by Zhao and Faltinsen [22], Nossen et al. [23], Grue and Biberg [24] and Teng and Taylor [25] in the frequency domain and Isaacson and Cheung [26], Cheung et al. [27], Liu et al. [28], Feng and Price [29] and Feng et al. [30] in the time domain. All these results illustrated that the uniform current will remarkably change the value of linear wave elevation and force on the structures. For nonlinear problems, we can solve them through the second order theory or fully nonlinear theory. Büchmann et al. [31] studied the second order wave diffraction by a single isolated bottom-mounted vertical cylinder and obtained the run-ups around the cylinder. Skourup et al. [32] then analysed the wave forces in the same cases as those in Büchmann et al. [31]. Their results further demonstrated that the second-order wave and force are clearly affected by the current. Other studies about interaction between Stokes second order wave and single-structure included those by Shao and Faltinsen [33, 34]. Researches about full nonlinear water waves and structures interaction in a uniform current included Büchmann et al. [35], Celebi [36], Ferrant [37] and Koo and Kim [38], and their results also show that hydrodynamic forces and wave elevation will be deeply affected by the current.

The works mentioned above are all about an isolated single structure in a current. However multi-structures are more common in practical ocean engineering and always show a complicated hydrodynamic characteristic such as Kim and Kim [39] who studied linear diffraction by four bottom-mounted cylinders. However, they did not consider the nonlinear effect and the influence of current on near-trapping phenomenon. This paper mainly aims to analyse the second order nonlinear interactions between water wave and four bottom mounted cylinders in a uniform current especially consider the situation at the near-trapped frequencies. In the present paper, we extend the work of Wang and Wu [15] to the wave diffraction by four-cylinders in a uniform current, and focus is on the near-trapping phenomenon under a current.

2. Theoretical formulation

2.1. *Boundary value problem*

The sketch of the wave diffraction by multi-cylinder is presented in Fig. 1. A right-handed Cartesian system $oxyz$ is defined with its origin o located at the centre of the configuration. The z-axis is positive upwards and the plane oxy is on the calm water surface. In this figure, S_f and S_b denote the free surface and the cylinder surface, respectively. The radius of the section of each cylinder is assumed to be identical and is expressed as a, and L_{cy} denotes the distance between two adjacent cylinders. The horizontal seabed is along $z = -h$.

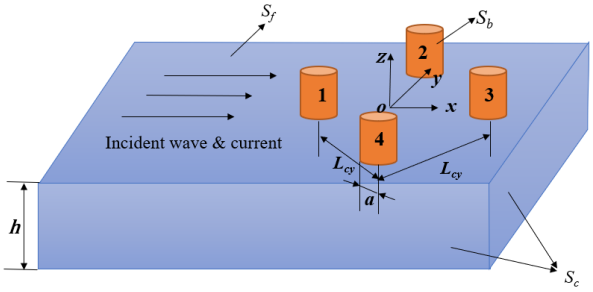

Fig. 1. Sketch of four-cylinder configuration in incident wave and current.

The fluid is assumed to be potential flow, a velocity potential $\phi(x, y, z)$ can be defined and used to describe the flow in the whole fluid domain Ω_f

$$\nabla^2\phi = 0. \tag{1}$$

The free surface boundary conditions including the kinematic and the dynamic be written as

$$\frac{\partial\phi}{\partial z} - \frac{\partial\eta}{\partial t} - \frac{\partial\phi}{\partial x}\frac{\partial\eta}{\partial x} - \frac{\partial\phi}{\partial y}\frac{\partial\eta}{\partial y} = 0 \qquad \text{on } S_f, \tag{2}$$

$$\frac{\partial\phi}{\partial t} + g\eta + \frac{1}{2}|\nabla\phi|^2 = 0 \qquad \text{on } S_f, \tag{3}$$

respectively, where t represents the time, η the wave elevation and g gravitational acceleration. The boundary conditions on cylinder surface and seabed is expressed as

$$\frac{\partial\phi}{\partial n} = 0 \qquad \text{on} \quad S_b, \tag{4}$$

$$\frac{\partial\phi}{\partial z} = 0 \qquad \text{on} \quad z = -h, \tag{5}$$

where $\vec{n} = (n_x, n_y, n_z)$ denotes the unit normal vector on S_b with its direction outward the fluid domain.

The perturbation method is applied to solve this question. The velocity potential and wave elevation can be expanded to second order, respectively

$$\phi = \phi_c + \varepsilon\phi^{(1)} + \varepsilon^2\phi^{(1)} = \phi_c + \varepsilon\left(\phi_I^{(1)} + \phi_D^{(1)}\right) + \varepsilon^2(\phi_I^{(1)} + \phi_D^{(1)}), \tag{6}$$

$$\eta = \varepsilon\eta^{(1)} + \varepsilon^2\eta^{(2)} = \varepsilon(\eta_I^{(1)} + \eta_D^{(1)}) + \varepsilon^2(\eta_I^{(2)} + \eta_D^{(2)}), \tag{7}$$

where, ε is a small parameter and chosen to be the linear wave slope. $\phi^{(i)}$ $(i = 1, 2)$ represents the i-th order velocity potential and $\eta^{(i)}$ $(i = 1,2)$ the i-th order wave elevation. The subscripts I and D mean the incident and diffraction wave components respectively. The

velocity potential ϕ_c can be further split into $\phi_c = Ux + \phi^{(0)}$, where U is the uniform current speed and $\phi^{(0)}$ is the disturbed potential due to the interaction between the current and cylinders.

The Taylor expansion is employed to deal with the free surface conditions given in Eqs. (2) and (3)

$$(\frac{\partial\phi}{\partial z} - \frac{\partial\eta}{\partial t} - \frac{\partial\phi}{\partial x}\frac{\partial\eta}{\partial x} - \frac{\partial\phi}{\partial y}\frac{\partial\eta}{\partial y}) + \eta\frac{\partial}{\partial z}(\frac{\partial\phi}{\partial z} - \frac{\partial\eta}{\partial t} - \frac{\partial\phi}{\partial x}\frac{\partial\eta}{\partial x} - \frac{\partial\phi}{\partial y}\frac{\partial\eta}{\partial y}) + \cdots|_{z=0} = 0, \tag{8}$$

$$(\frac{\partial\phi}{\partial t} + g\eta + \frac{1}{2}|\nabla\phi|^2) + \eta\frac{\partial}{\partial z}(\frac{\partial\phi}{\partial t} + g\eta + \frac{1}{2}|\nabla\phi|^2) + \cdots|_{z=0} = 0. \tag{9}$$

With the application of perturbation theory, this problem can be decomposed into two subproblems: one is to solve the disturbed potential $\phi^{(0)}$ with omitting the wave effect and the other is to calculate the *i*-th (*i*=1, 2) order diffraction potentials.

The governing equation and boundary condition of $\phi^{(0)}$ can be described by:

$$\nabla^2\phi^{(0)} = 0 \quad \text{in } \Omega_f^{(0)}, \tag{10}$$

$$\frac{\partial\phi^{(0)}}{\partial n} = -Un_x \quad \text{on } S_b^{(0)}, \tag{11}$$

where $\Omega_f^{(0)}$ is a fixed fluid domain below the calm water level $z = 0$, $S_b^{(0)}$ denotes the cylinder surface below $z = 0$. The diffraction potential also satisfies the Laplace equation

$$\nabla^2\phi_D^{(k)} = 0\ (k = 1, 2) \quad \text{in } \Omega_f^{(0)}, \tag{12}$$

and the corresponding boundary conditions on the free surface are given as

$$\frac{\partial\phi_D^{(k)}}{\partial z} - \frac{\partial\eta_D^{(k)}}{\partial t} = f_k' \quad \text{on } z = 0, \tag{13}$$

$$\frac{\partial\phi_D^{(k)}}{\partial t} + g\eta_D^{(k)} = f_k'' \quad \text{on } z = 0. \tag{14}$$

In Eqs. (13) and (14), the right-hand sides terms are, respectively,

$$f_1' = \left(U + \frac{\partial\phi^{(0)}}{\partial x}\right)\frac{\partial\eta^{(1)}}{\partial x} + \frac{\partial\phi^{(0)}}{\partial y}\frac{\partial\eta^{(1)}}{\partial y} + \eta^{(1)}\frac{\partial^2\phi^{(0)}}{\partial z^2} - (\frac{\partial\phi_I^{(1)}}{\partial z} - \frac{\partial\eta_I^{(1)}}{\partial t}),$$

$$f_2' = \frac{\partial\phi^{(1)}}{\partial x}\frac{\partial\eta^{(1)}}{\partial x} + \frac{\partial\phi^{(1)}}{\partial y}\frac{\partial\eta^{(1)}}{\partial y} - \eta^{(1)}\frac{\partial^2\phi^{(1)}}{\partial z^2} - \eta^{(2)}\frac{\partial^2\phi^{(0)}}{\partial z^2} + \left(U + \frac{\partial\phi^{(0)}}{\partial x}\right)\frac{\partial\eta^{(2)}}{\partial x} +$$

$$\frac{\partial\phi^{(0)}}{\partial y}\frac{\partial\eta^{(2)}}{\partial y} - (\frac{\partial\phi_I^{(2)}}{\partial z} - \frac{\partial\eta_I^{(2)}}{\partial t}),$$

$$f_1'' = -(U + \frac{\partial\phi^{(0)}}{\partial x})\frac{\partial\phi^{(1)}}{\partial x} - \frac{\partial\phi^{(0)}}{\partial y}\frac{\partial\phi^{(1)}}{\partial y} - (\frac{\partial\phi_I^{(1)}}{\partial t} + g\eta_I^{(1)}),$$

$$f_2'' = -\frac{1}{2}\left|\nabla\phi^{(1)}\right|^2 - \eta^{(1)}\left[\frac{\partial\phi^{(1)}}{\partial z}\frac{\partial^2\phi^{(0)}}{\partial z^2} + \frac{\partial^2\phi^{(1)}}{\partial z\partial t} + \left(U + \frac{\partial\phi^{(0)}}{\partial x}\right)\frac{\partial^2\phi^{(1)}}{\partial x\partial z} + \frac{\partial\phi^{(0)}}{\partial y}\frac{\partial^2\phi^{(1)}}{\partial y\partial z}\right] -$$

$$(U + \frac{\partial\phi^{(0)}}{\partial x})\frac{\partial\phi^{(2)}}{\partial x} - \frac{\partial\phi^{(0)}}{\partial y}\frac{\partial\phi^{(2)}}{\partial y} - (\frac{\partial\phi_I^{(2)}}{\partial t} + g\eta_I^{(2)}).$$

Correspondingly, other boundary conditions are

$$\frac{\partial\phi_D^{(k)}}{\partial n} = -\frac{\partial\phi_I^{(k)}}{\partial n} = -\vec{n}\cdot\nabla\phi_I^{(k)} \quad \text{on } S_b^{(0)}, \tag{15}$$

$$\frac{\partial \phi_D^{(k)}}{\partial z} = 0 \quad \text{on } z = -h. \tag{16}$$

The analytical solution of the incident wave elevations and velocity potentials to second-order can be expressed as, respectively

$$\eta_I^{(1)} = \frac{H}{2}\cos\theta, \tag{17}$$

$$\phi_I^{(1)} = \frac{Hg}{2\omega}\frac{\cosh k(z+h)}{\cosh(kh)}\sin\theta, \tag{18}$$

$$\eta_I^{(2)} = -\frac{H^2 k}{8\sinh(2kh)} + \frac{H^2 k\cosh(kh)[2\cosh^2(kh)+1]}{16\,sinh^3(kh)}\cos 2\,\theta, \tag{19}$$

$$\phi_I^{(2)} = \frac{3H^2\omega\cosh 2k(z+h)}{32\sinh^4(kh)}\sin 2\theta, \tag{20}$$

where k and H represents the linear wave number and linear wave height respectively, ω the linear frequency without the effect of current and it can be calculated by equation$\omega = \sqrt{kg\tanh(kh)}$. In above equations, $\theta = kx - \omega_c t$, where ω_c denotes the encounter frequency of linear wave and can be determined by $\omega_c = \omega + Uk$.

2.2. Evaluation of hydrodynamic forces

The Bernoulli equation is employed to obtain the pressure in any position in the fluid domain,

$$p = -\rho(\frac{\partial \phi}{\partial t} + \frac{1}{2}\nabla\phi\cdot\nabla\phi + gz), \tag{21}$$

where ρ is the density of water. The hydrodynamic force and moment on any cylinder can be determined through the integral of pressure over the cylinder surface

$$\vec{F} = \iint_{S_b} p\vec{n}\,ds, \tag{22}$$

$$\vec{M} = \iint_{S_b} p(\vec{r}\times\vec{n})\,ds, \tag{23}$$

where $\vec{r} = (x - x_c, y - y_c, -h)$ and $(x_c,\ y_c)$ is the centre of each cylinder section. The force can be further split into the sum of the first-order oscillatory force$\vec{F}^{(1)}$, the second-order oscillatory force $\vec{F}^{(2)}$and the second order mean drift force $\bar{\vec{F}}^{(2)}$

$$\vec{F} = \vec{F}^{(1)} + \vec{F}^{(2)} + \bar{\vec{F}}^{(2)}, \tag{24}$$

Where

$$\vec{F}^{(1)} = -\rho\iint_{S_b^{(0)}}(\frac{\partial \phi^{(1)}}{\partial t} + \nabla\phi_c\cdot\nabla\phi^{(1)})\vec{n}ds, \tag{25}$$

$$\vec{F}^{(2)} = -\rho\iint_{S_b^{(0)}}(\frac{\partial \phi^{(2)}}{\partial t} + \frac{1}{2}\nabla\phi^{(1)}\cdot\nabla\phi^{(1)} + \nabla\phi_c\cdot\nabla\phi^{(2)})\vec{n}ds + \frac{1}{2}\rho g\oint_l[\eta^{(1)}]^2\vec{n}dl - \bar{\vec{F}}^{(2)}, \tag{26}$$

$$\bar{\vec{F}}^{(2)} = -\frac{1}{2}\rho\,\overline{\iint_{S_b^{(0)}}(\nabla\phi^{(1)}\cdot\nabla\phi^{(1)} + 2\nabla\phi_c\cdot\nabla\phi^{(2)})\vec{n}ds} + \frac{1}{2}\rho g\,\overline{\oint_l[\eta^{(1)}]^2\vec{n}dl}, \tag{27}$$

where l denotes the mean waterline of the cylinder. The calculation of moments$\vec{M}^{(1)}$, $\vec{M}^{(2)}$

and $\vec{M}^{(2)}$ is similar with Eqs. (25)~(27), respectively.

3. Numerical method and Procedures

The finite element method is adopted in this paper. The three-dimensional (3-D) prismatic element with 6-node will be applied in the simulation, which is produced by vertically extending a horizontal plane with 2-D unstructured mesh. The mesh generation codes named BAMG Hecht [40] is employed to generate the 2-D unstructured triangular mesh. Normally, the disturbance caused by water waves has rapid attenuation along the water depth, and hence the elements need be smaller near the water surface and then gradually become larger along the water depth, which is achieved by employing the method in Chung [41] and it has been used by Wang and Wu [15].

With the application of FEM, the velocity potential can be obtained through the linear superposition of the node value

$$\phi^{(k)} = \mathbf{N}^T \Phi^{(k)}, \quad (k = 0, 1, 2), \tag{28}$$

where $\mathbf{N}$ is the shape function vector, Φ is the potential vector. The velocity potential can be obtained through solving the linear systems

$$\mathbf{K}\Phi^{(k)} = \mathbf{F}^{(k)}, \quad (k = 0, 1, 2), \tag{29}$$

where the coefficient matrix is represented by $\mathbf{K}$, the right-hand side vector is represented by $\mathbf{F}$. The elements of $\mathbf{K}$ and $\mathbf{F}$ can be calculated by the following equations,

$$K_{ij} = \iiint_{\Omega_f^{(0)}} \nabla N_i \cdot \nabla N_j d\Omega \quad (i \notin S_p, j \notin S_p), \tag{30}$$

$$F_i^{(k)} = \iint_{S_n} N_i f_n^{(k)} dS - \iiint_{\Omega_f^{(0)}} \nabla N_i \sum_{j(j \in S_p)} (f_p^{(k)})_j \nabla N_j d\Omega \quad i \notin S_p, \tag{31}$$

where S_p denotes the Dirichlet boundary of potentials and $f_p^{(k)}(k = 0, 1, 2)$ the value of $\phi^{(k)}$ on S_p. S_n is the Neumann boundary where the value of $\partial\phi^{(k)}/\partial n$ is specified and is represented by $f_n^{(k)}(k = 0, 1, 2)$. The linear systems of Eq. (29) can be efficiently solved by an iteration method based on the preconditioned conjugate gradient algorithm to obtain the potentials.

The wave and velocity potential on the free surface are updated through calculating the integration with respect to time by the fourth-order Adams-Bashforth scheme, which can be written as $f(t + \Delta t) = f(t) + \Delta t[55f'(t) - 59f'(t - \Delta t) + 37f'(t - 2\Delta t) - 9f'(t - 3\Delta t)]/24$ ($f'(t)$ is the derivative of $f(t)$).

The damping zone method is applied to absorb the waves near the open boundary S_c, which can be achieved by adding a damping term named Newtonian cooling term to the kinematic boundary condition Eq. (13),

$$\frac{\partial \eta_D^{(k)}}{\partial t} = \frac{\partial \phi_D^{(k)}}{\partial z} - f_k' - 2\nu\eta_D^{(k)} + \frac{\nu^2}{g}\phi_D^{(k)} \quad (k = 1,2) \quad \text{on } z = 0, \tag{32}$$

where ν denotes the damping coefficient and is calculated through

$$\nu(d) = 3\frac{C_s}{C_w^3}(d - d_0)^2 \quad 0 \le d - d_0 \le C_w$$

(33)

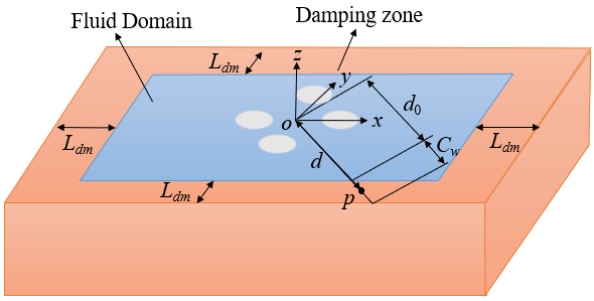

Fig. 2. Sketch of damping zone.

where d is the distance between the any point p on the mean free surface and the centre of the nearest cylinder. The damping zone is presented in Fig.2 and is bounded by two rectangular domains: the inner $d = d_0(x, y)$ and the outer $d = d_0(x, y) + C_w(x, y)$. The constant C_s in Eq. (33) is used for controlling the strength of $\nu(d)$ and chosen as 1.0 in the simulation. The width of the damping zone is denoted by L_{dm}, which can be chosen to be one linear wavelength for long waves and twice linear wavelength for short waves.

Although the velocity at nodes can be directly calculated through the derivative of the shape function, but it is not sufficiently accurate for linear elements due to the fact that the value of velocity will be constant on the facet. The method developed by Ma et al. [42, 43] will be applied to obtain the velocity component in the z-direction at nodes on the free surface. The corresponding horizontal velocity components can then be obtained through differencing the velocity potential. The term $\nabla\phi$ over the body surface used for calculating forces can be determined through the shape function directly which was applied by Wang and Wu [15].

4. Numerical results

To allow a gradual development of the diffraction potential and avoid an abrupt start, a modulation or ramp function is employed to the cylinder surface condition given in Eq. (15)

$$\frac{\partial \phi_D^{(k)}}{\partial n} = -M(t)\frac{\partial \phi_I^{(k)}}{\partial n} \quad (k = 1,2), \tag{34}$$

where $M(t)$ can be obtained by:

$$M(t) = \begin{cases} \frac{1}{2}[1 - \cos(\frac{\pi t}{T})] & t < T \\ 1 & t \geq T \end{cases}$$

where $T = 2\pi/\omega$ is the period of the first-order incident wave.

The linear wave slope H/L is chosen to be 0.025 in the present study, therefore $kA = \pi/40$, where L is the wavelength of the linear incident wave, $A = H/2$ is the linear wave amplitude. The nondimensional wavenumber is denoted by ka and the current speed is nondimensionalized by Froude number $Fr = U/\sqrt{ga}$.

4.1. Single column case

Before simulating four-cylinder cases, a single isolated cylinder whose centre is at the origin and the initial water depth $h = a$ is considered for validation. The results about the amplitudes of second order force & moment versus the nondimensional wavenumber ka are

given in Figs. 3a and 3b respectively. In the figure, F & M are the force & moment and the subscripts x & y express their components along the x- and y- directions, respectively, and hereinafter in the subsequent figures. We made a comparison between our numerical results and those obtained by Skourup et al. [32]. It is seen from the Fig. 3 that they are in a great agreement.

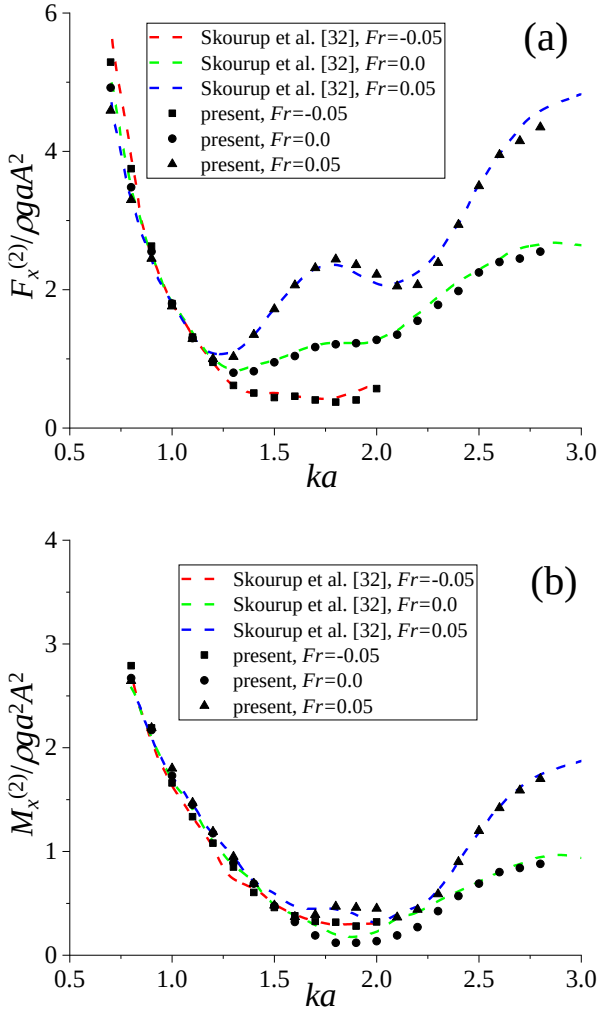

Fig. 3. Second order force and moment versus *ka*; (a) amplitude of second order oscillatory force; (b) amplitude of second order oscillatory moment.

4.2. Four-column case

The simulation is then made for wave diffraction by four vertical seabed-mounted cylinders with neighbouring spacing $L_{cy} = 6a$ and calm water depth $h = a$ (see Fig 6a), which has also been investigated by Kim and Kim [39] using the linear theory. A comparison between the total hydrodynamic forces on all cylinders obtained by Kim and Kim [39] through a higher order panel element method and the present FEM results is shown in Figs. 4 and Fig. 5, respectively. Fig. 4 shows the amplitudes of linear force and moment while Fig. 5 is the second-order mean drift force. Three Froude numbers $Fr = -0.04,\ 0\ \&\ 0.04$ are used in the simulations. They agree well with each other and there is slight difference only at some ka, which further confirms the present numerical method is effective.

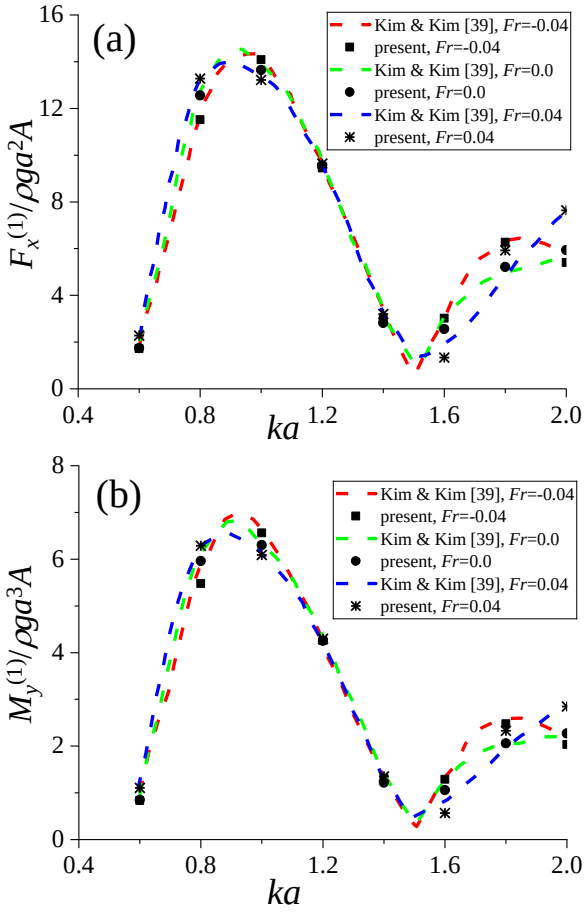

Fig. 4. The amplitude of total first-order force and moment on four cylinders versus *ka*.

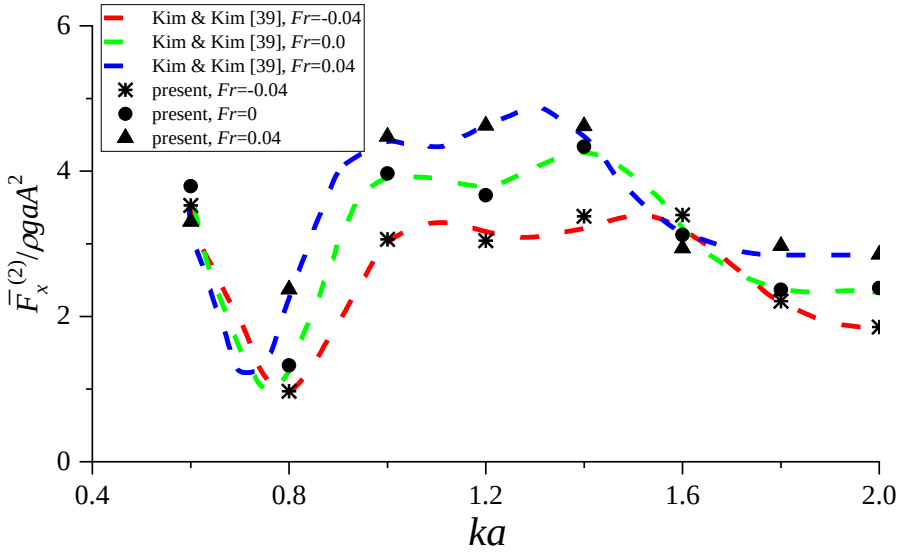

Fig. 5. Total second-order mean drift forces on four cylinders versus *ka*.

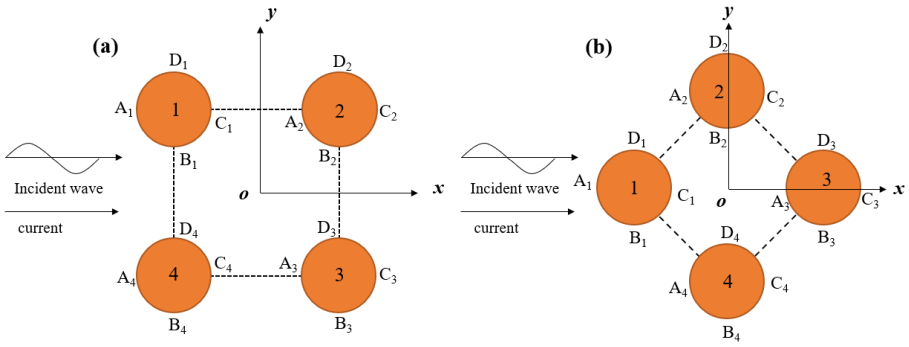

Fig. 6. Sketch of two four-cylinder configurations.

4.2.1. Numerical simulation of Four-column case (a)

We turn to the four-cylinder configuration shown in Fig. 6a but with $L_{cy} = 4a$ and $h = 3a$. The propagation direction of incident wave is along the positive x-axis while the steady current is in the same or reverse direction. The three Froude numbers mentioned above are also used. Fig. 7 shows the linear wave amplitude versus ka. It can be found that the wave amplitude is affected by the current clearly. However, the amplitude fluctuates as ka at each Froude number due to the wave interference produced by the cylinders and hence they are different from those in a single cylinder case (see Fig. 8), in which the wave amplitude regularly increases as Fr increases at each ka. For the second-order wave given in Fig. 9, from which we can find the wave amplitudes at all Froude numbers fluctuate even more seriously.

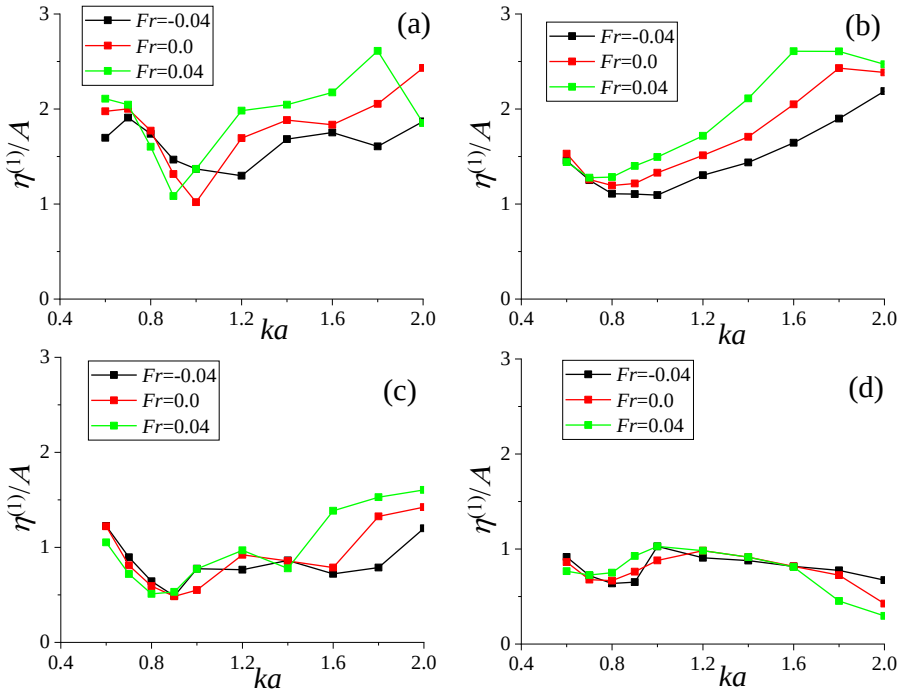

Fig. 7. The amplitude of linear wave elevation versus ka under three different Fr;
(a) front side of cylinder 1; (b) front side of cylinder 2;
(c) back side of cylinder 1; (d) back side of cylinder 2.

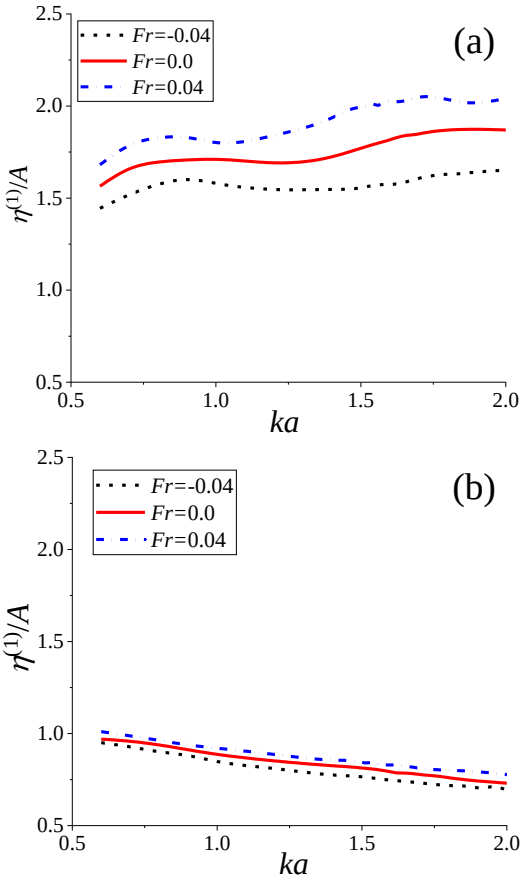

Fig. 8. Linear wave amplitude of a single isolated cylinder;
(a) front side; (b) back side

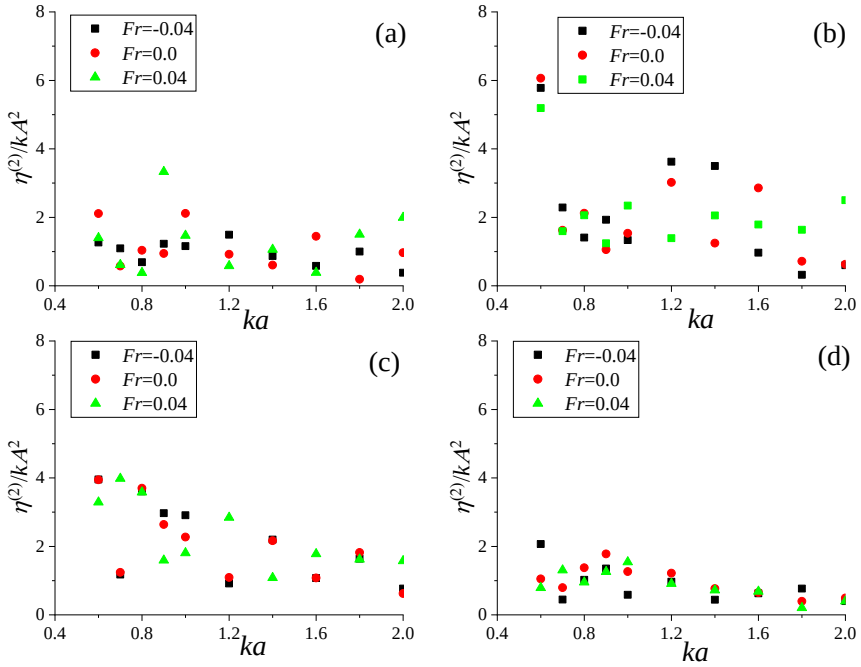

Fig. 9. The amplitude of second order wave elevation versus *ka* under three different *Fr*;
(a) front side of cylinder 1; (b) front side of cylinder 2;
(c) back side of cylinder 1; (d) back side of cylinder 2.

Fig. 10 presents the amplitudes of the linear forces on cylinders 1 & 2. When compared with the linear wave, it seems that the influence of the current on the force is relatively smaller. However, it is significant for the second order force (see Fig. 11). The maximum value of the linear forces appears at ka=0.6 & Fr=0 (see Fig. 10a) and it is 7.9. The second order force amplitude has a dramatic increase at $ka = 2$ when Fr changes from 0 to 0.04 and it reaches a peak about 12.6.

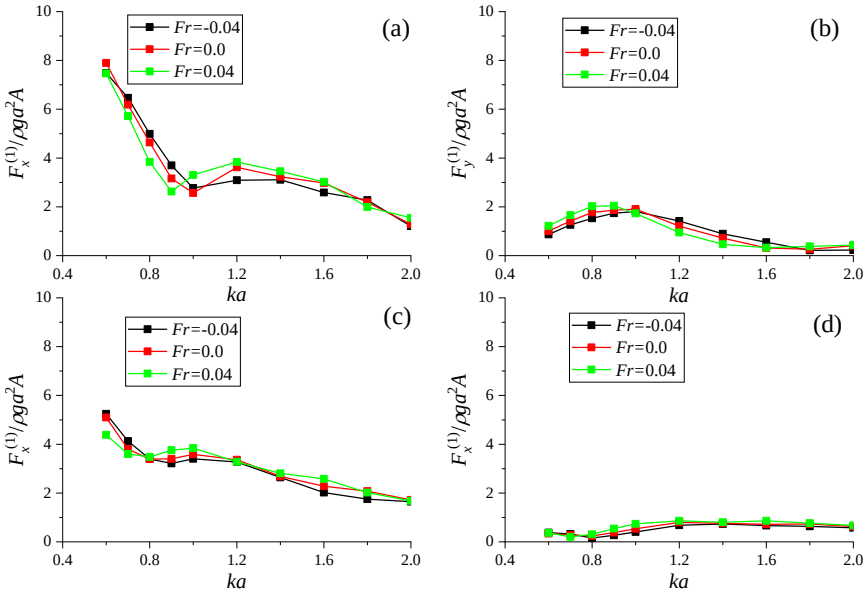

Fig. 10. The amplitude of first-order forces versus ka under three different Fr; (a) & (b) cylinder 1; (c) & (d) cylinder 2.

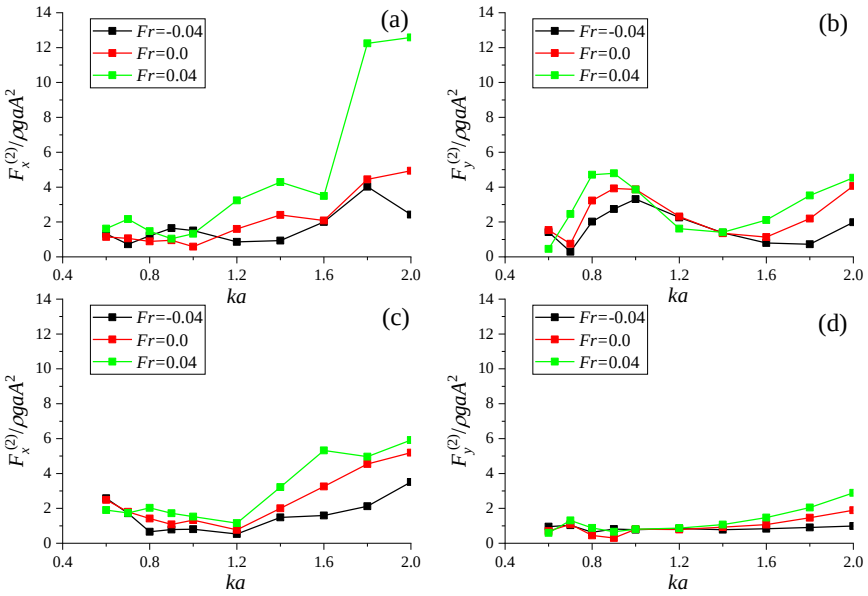

Fig. 11. The amplitude of second-order forces versus ka under three different Fr; (a) & (b) cylinder 1; (c) & (d) cylinder 2.

4.2.1. Numerical simulation of Four-column case (b)

The wave elevations and hydrodynamic forces on cylinders will be quite different between

the four-cylinder configurations Figs. 6a and 6b. As described by Evans and Porter [13] and Malenica et al. [14], one of the most interesting things in Fig. 6b is the near-trapping phenomenon, when the wave frequency approaches the trapped frequency, the wave elevation at some locations and hydrodynamic force on the cylinders become very large. Through frequency domain analysis, they found that the first- and second-order near-trapping phenomenon happen at about ka equals to 1.66 and 0.468, respectively. In the present paper, we consider the near-trapped modes under uniform currents. In the simulation of configuration in Fig. 6b, the calm water depth is also $h = 3a$ and the spacing between neighbouring cylinders is $L_{cy} = 4a$ too.

The linear wave elevations at four positions A_1, C_1, B_2 and A_3 (see Fig. 6b) are firstly calculated and the results about the amplitude versus ka is given in Fig. 12. The time interval in the simulation is chosen to be $T/200$ for Fr=0 and $T/400$ for Fr=-0.04 & 0.04. The numbers of nodes and elements are listed in Table 1, in which NC is the intervals along the intersection line between each cylinder and the still water surface, NH is the layer number along the vertical direction, and NE & NN are the numbers of the total elements & nodes in the fluid domain, respectively. It can be found from the Fig. 12 that the uniform current has relatively little influence on the wave at these four points within ka<1.2. When ka>1.2, the curves at three Froude numbers are significantly different and there exist some maximum wave amplitudes especially in Figs. 12b and 12d, which may correspond to the near-trapping phenomenon. As Evans and Porter [13] pointed out, the wave energy is concentrated within the region of four cylinders especially near points C_1 and A_3. It can be seen that the peaks of the wave amplitudes at Fr=-0.04, 0.0 & 0.04 occur at ka=1.88, 1.66 & 1.52, respectively, which correspond to encounter frequencies 4.059, 4.035 & 4.052, respectively, through equation $\omega_c = \omega + Uk$. Theoretically, these encounter frequencies should be identical to each other. However, there is slight difference between them in actual numerical simulations.

ka	*NH*	*NC*	*NN*	*NE*
0.6	14	32	187140	343028
0.8	14	36	195930	359212
1.0	14	40	196080	359436
1.2	14	40	177135	324184
1.4	14	40	172305	315056
1.6	14	40	158085	288624
1.8	14	44	157800	287868
2.0	14	44	149550	272580

Table 1 Numbers of element and nodes at different *ka*.

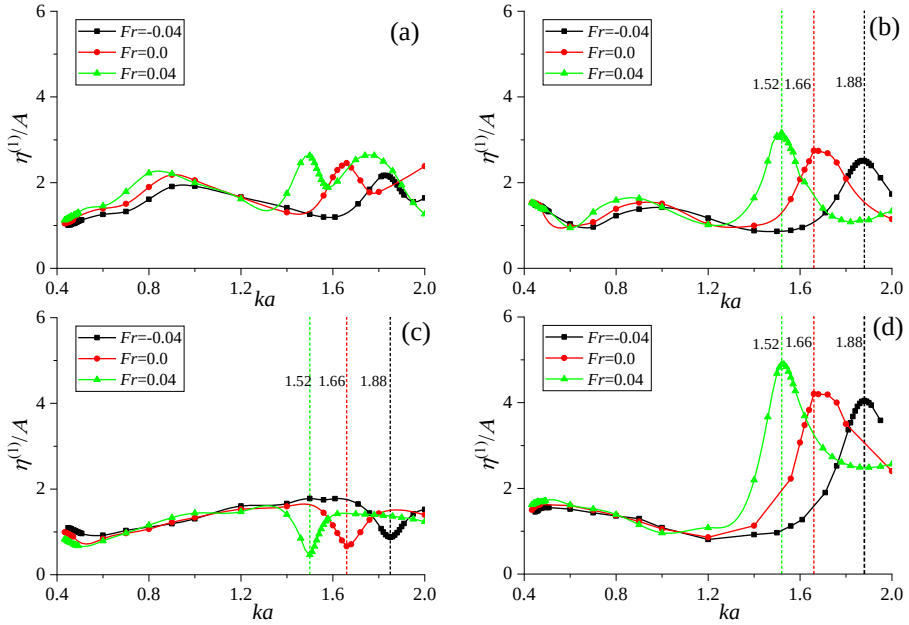

Fig. 12. The amplitude of linear wave elevation versus *ka* under three different *Fr*; (a) A_1; (b) C_1; (c) B_2; (d) A_3

The linear wave amplitude clearly increases as *Fr* increases at four positions especially at C_1 and A_3 at the near-trapping frequency, which indicates that the linear wave resonance phenomenon will be intensified when *Fr* increases. This is completely different from that found by Huang and Wang [44], in which the resonant wave produced by two cylinders in forced motions generally becomes weaker as *Fr* increases. However, the increase of wave amplitudes at A_1 and B_2 is not as large as those at C_1 & A_3. At *Fr*=-0.04, 0 & 0.04, the wave amplitudes are 2.51, 2.75 & 3.06 at C_1 and are 4.08, 4.21 & 4.90 at A_3, respectively, which is obviously larger than those in the single cylinder cases given in Fig. 9. Fig. 13 further states that the increase of the current speed causes the linear wave amplitude to increase with adding another two Froude numbers *Fr*=-0.02 & 0.02 to the simulation.

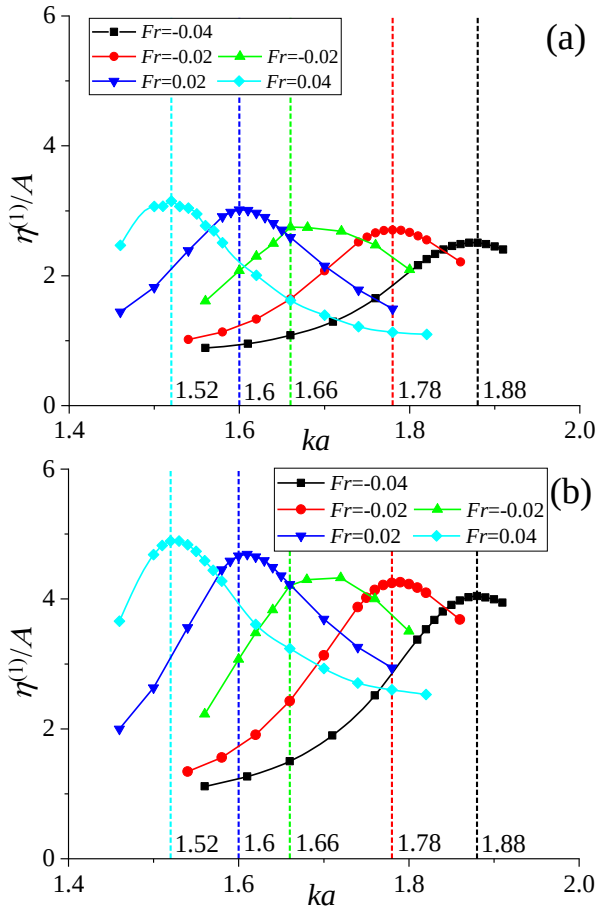

Fig. 13. The amplitude of linear wave elevation when *ka* is at near-trapping frequency; (a) A_3; (b) C_1.

The second-order wave amplitudes at the four positions mentioned above are presented in Fig. 14. The corresponding second-order wave amplitudes under second-order near-trapping phenomenon is quite obvious, and at C_1 & A_3 quickly increase when the wave frequency approaches the trapped frequency. It can be seen from the Figs. 14b and 14d that when *Fr*=-0.04. 0.0 & 0.04 the near-trapping phenomenon occurs at *ka*=0.488, 0.468 and 0.448 respectively. However, one thing different from the first-order near-trapping phenomenon is that the second-order wave amplitude at A_3 is much larger than that at C_1. The second-order wave amplitude at A_3 under three Froude number are 14.80, 16.61 & 17.14 respectively, almost twice those at C_1, which means that the second-order trapped is also intensified when the Froude number increases. Fig. 15 shows the peaks and troughs of resultant waves of the linear and the second-order. It is shown that the peak and trough at first-order trapped frequencies increase as *Fr* increases. At the second-order trapped frequencies, the trough at C_1 and peak at A_3 also clearly increase as *Fr* increases.

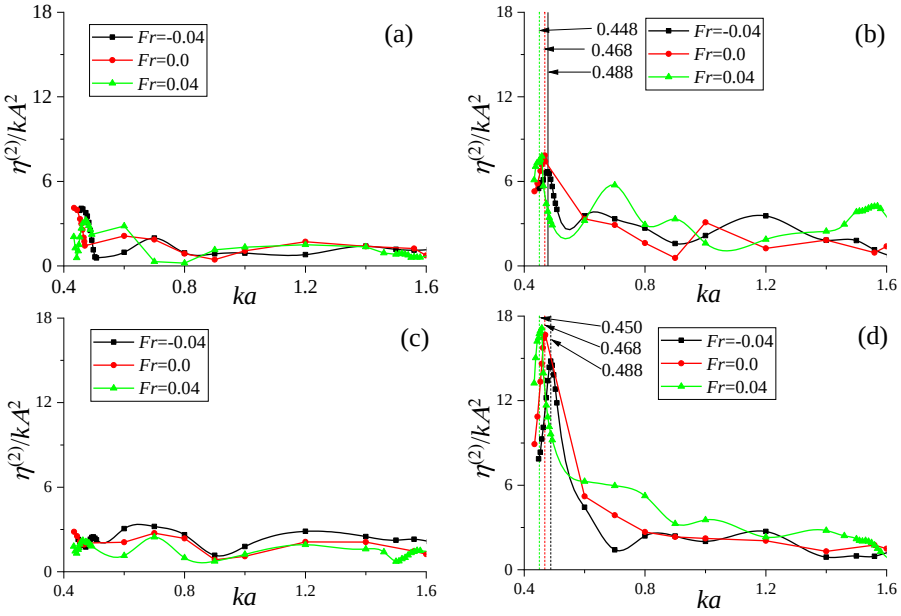

Fig. 14. The amplitude of second-order wave elevation versus *ka* under three different *Fr*: (a) A_1; (b) C_1; (c) B_2; (d) A_3

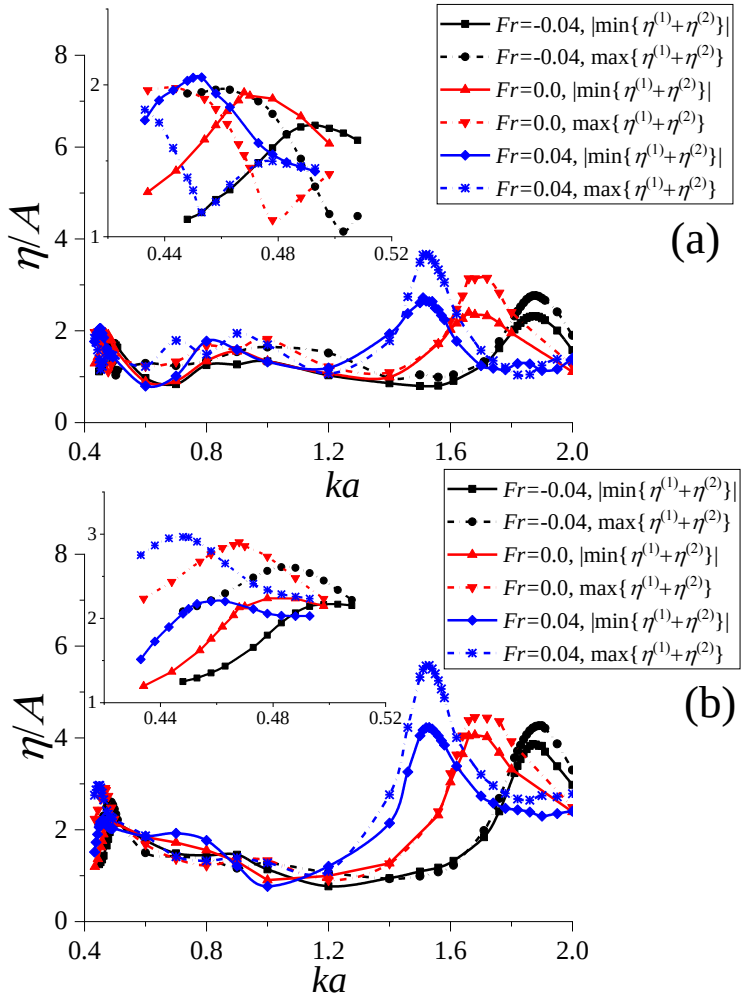

Fig. 15. Wave peaks and troughs versus *ka* under different *Fr*; (a) C_1; (b) A_3

The histories of linear and second-order waves at the first- and second-order near-trapped modes are presented in Figs. 16 and 17, respectively. It is shown from Fig. 16 that each wave finally reaches a steady state. The waves at different Froude numbers have clear difference and they are affected by the current in both amplitude and phase. Similarity can be found for the second wave given in Fig. 17.

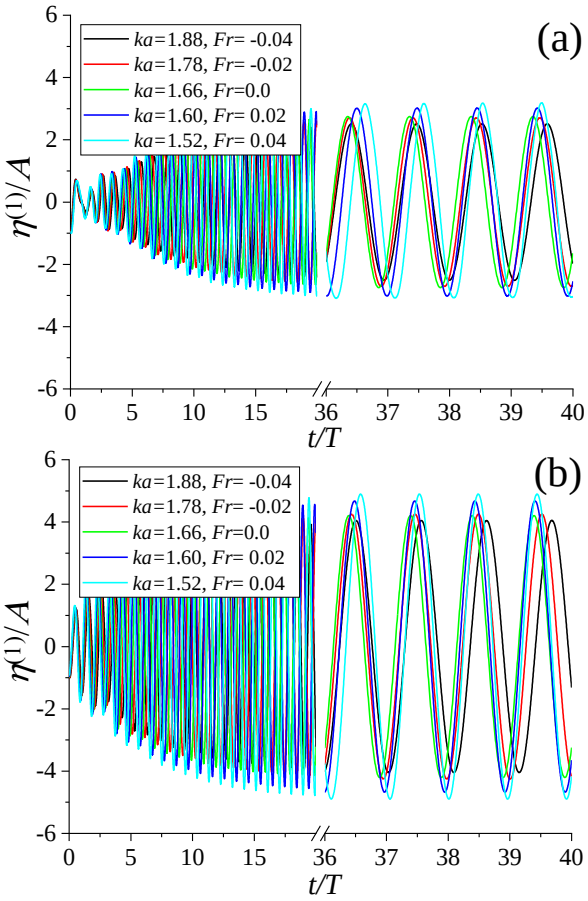

Fig. 16. Histories of linear wave at first-order near-trapped mode; (a) C_1; (b) A_3.

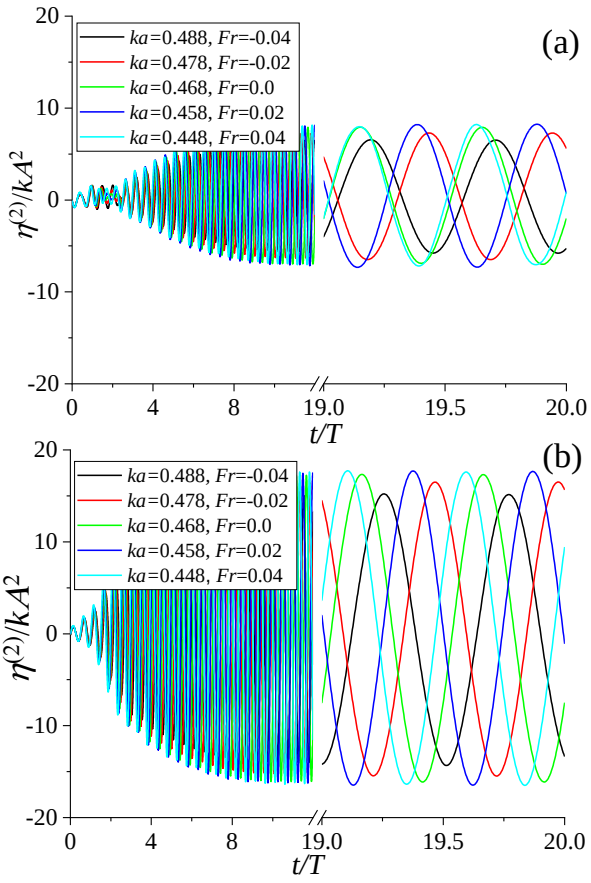

Fig. 17. Histories of second-order wave at second-order near-trapped mode; (a) C_1; (b) A_3.

Figs. 18 and 19 give the histories of linear wave and its superimposition with the second-order at the left and right sides of cylinders 1 & 3 at the first- and second-order near-trapped modes at Fr=0.04, respectively. It is noticed that the wave development with time becomes steady and the near-trapping phenomenon are clear due to larger linear waves at C_1 & A_3 in Fig. 18 and larger second order waves at C_1 & A_3 in Fig. 19. The wave profiles around the four cylinders at the second order near-trapped mode is plotted in Fig. 20. It can be observed that the difference between the linear wave and the resultant wave at each Fr is obvious due to second order effect. The superposed waves of linear and second order at different Fr are also very clear.

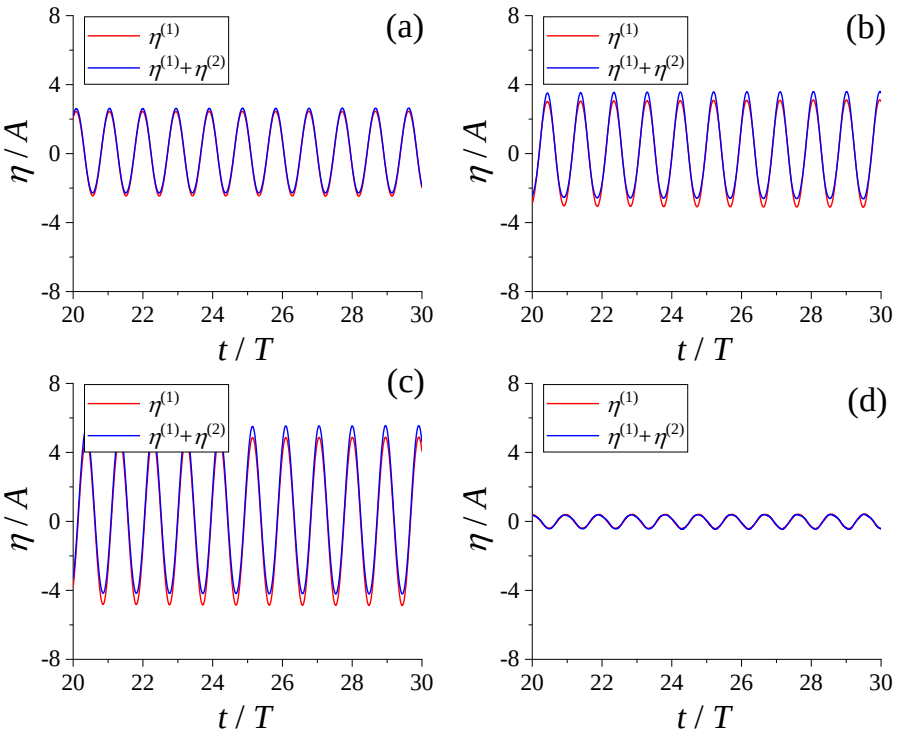

Fig. 18. Wave histories at ka=1.52, Fr=0.04: (a) A_1; (b) C_1; (c): A_3; (d) C_3.

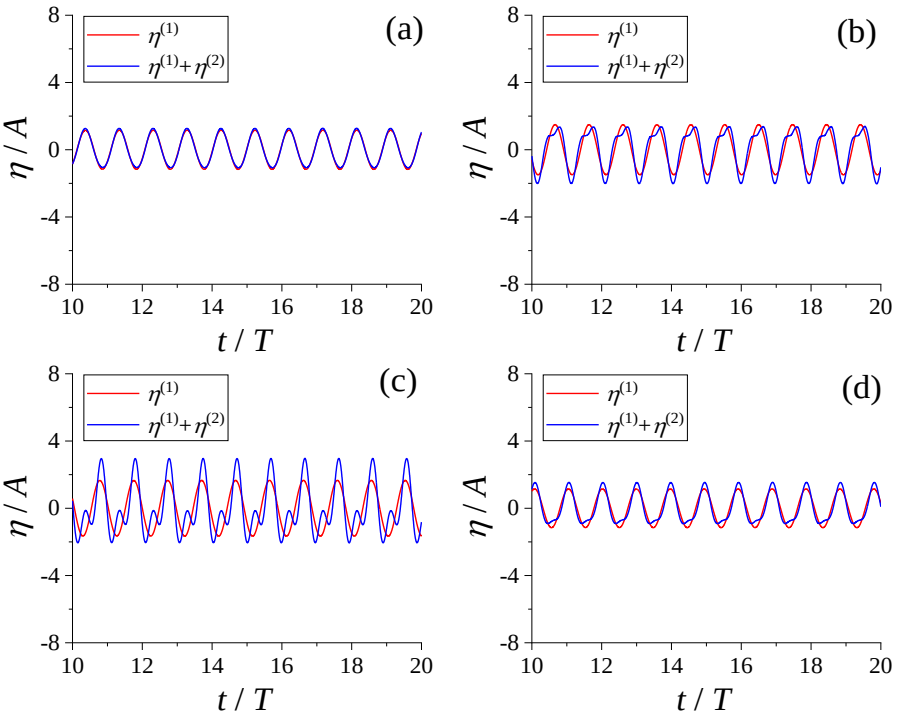

Fig. 19. Wave histories at ka=0.448, Fr=0.04: (a) A_1; (b) C_1; (c): A_3; (d) C_3.

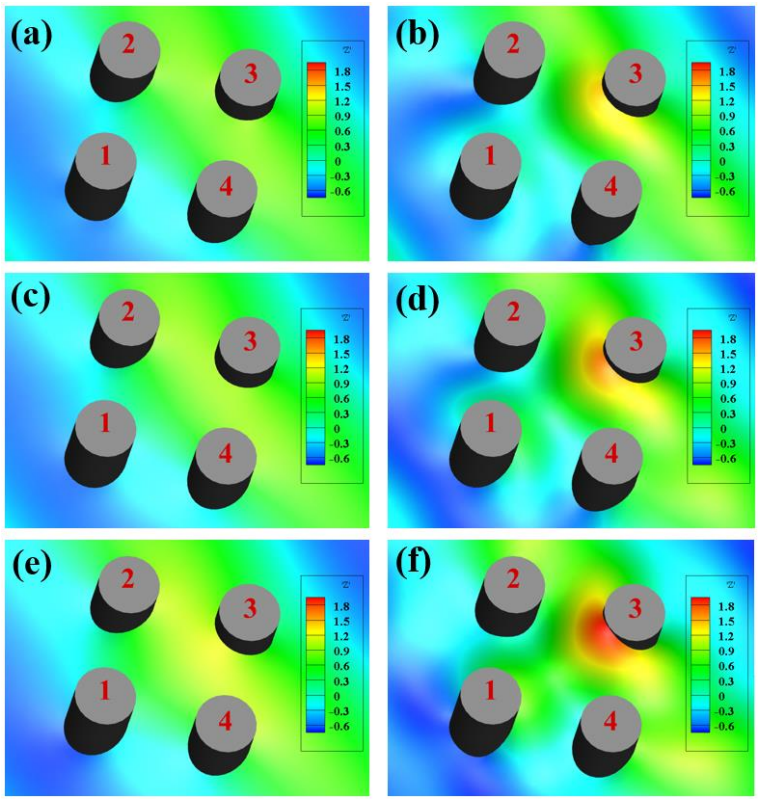

Fig. 20. Wave profiles around the four cylinders; (a) & (b): Fr=-0.04, ka=0.488, t/T=19.8; (a) & (d): Fr=0.0, ka=0.468, t/T=20.2; (e) & (f): Fr=0.04, ka=0.448, t/T=19.6; (a), (c) & (e): linear; (b), (d) & (f): linear plus second-order.

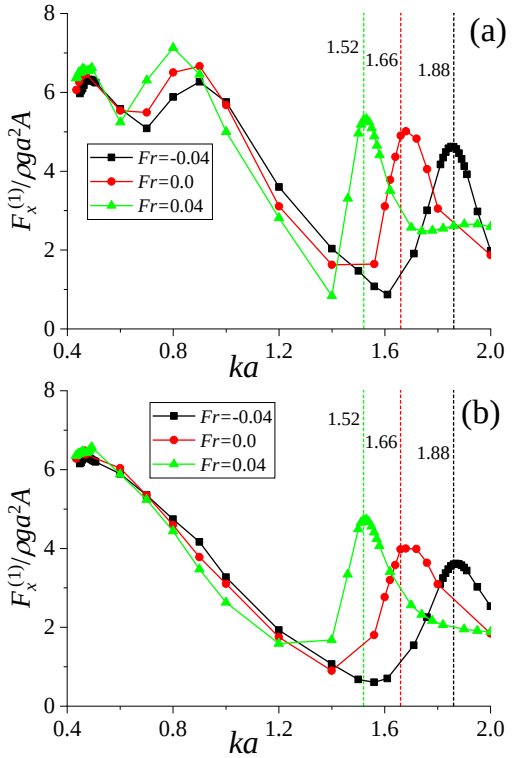

Fig. 21. The amplitude of first-order forces versus ka under three different Fr; (a) cylinder 1; (b) cylinder 2.

Fig. 21 gives the amplitude of linear forces on cylinders 1 & 3 at the first order near-trapped mode. We calculate the force in the *x*-direction only due to symmetry. It can be seen from Eq. (25) that the first-order force is affected by the first-order potential and the potential due to the current only. It can be seen that some features of the forces in Fig. 21 are similar to the waves in Figs. 11b & 11d. The variation of the force amplitude at each *Fr* with *ka* is different with that in a single isolated cylinder case given in Fig. 22. It can be noticed that the force peak at the near-trapping frequency increases as *Fr* and they are 4.62, 4.90 & 5.37 at *Fr*=-0.04, 0.0 & 0.04 for cylinder 1 and 3.60, 3.98 & 4.73 for cylinder 3, respectively.

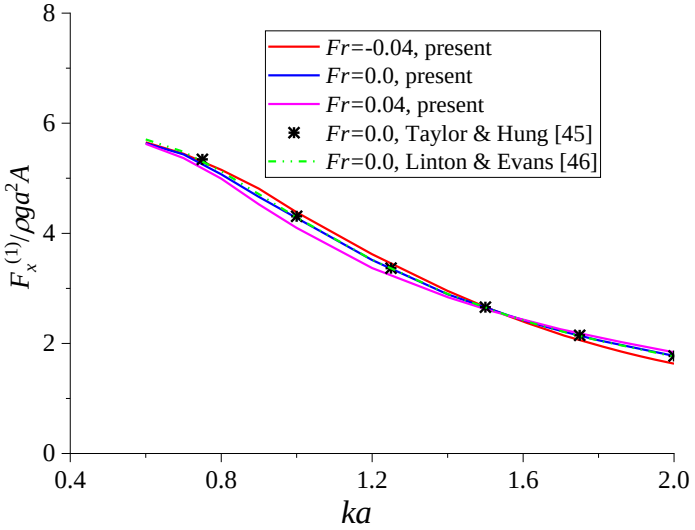

Fig. 22. The amplitude of first-order force of a single isolated cylinder versus *ka*.

Fig. 23 makes a comparison between linear forces in the present numerical simulations and with those by Evans and Porter [13] at $Fr = 0$. In the figure, $F_x^{(1)}/\mathbf{F}_s$ means the ratio of the linear force in the *x*-direction to a single isolated cylinder case and $\mathbf{F}_s = 4\rho g\rho \tanh(kh) / k^2 H_1'(ka)$, where H_1 is the first-kind Hankel function. The comparison shows that they are in good agreement for both cylinders.

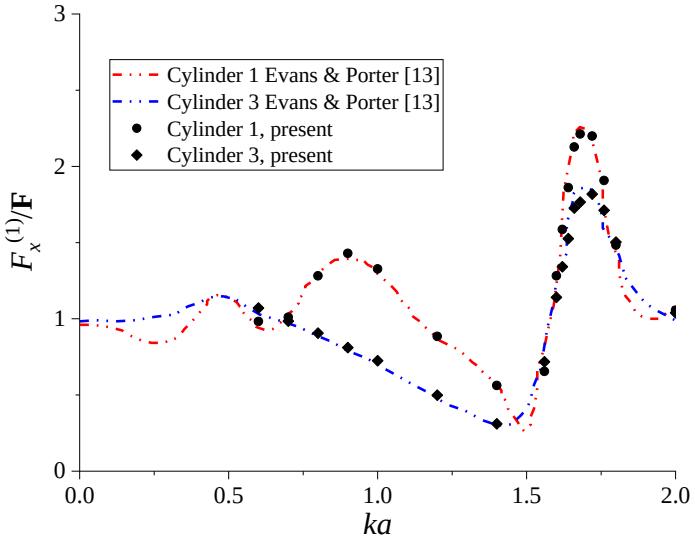

Fig. 23. A comparison of linear forces at *Fr*=0.

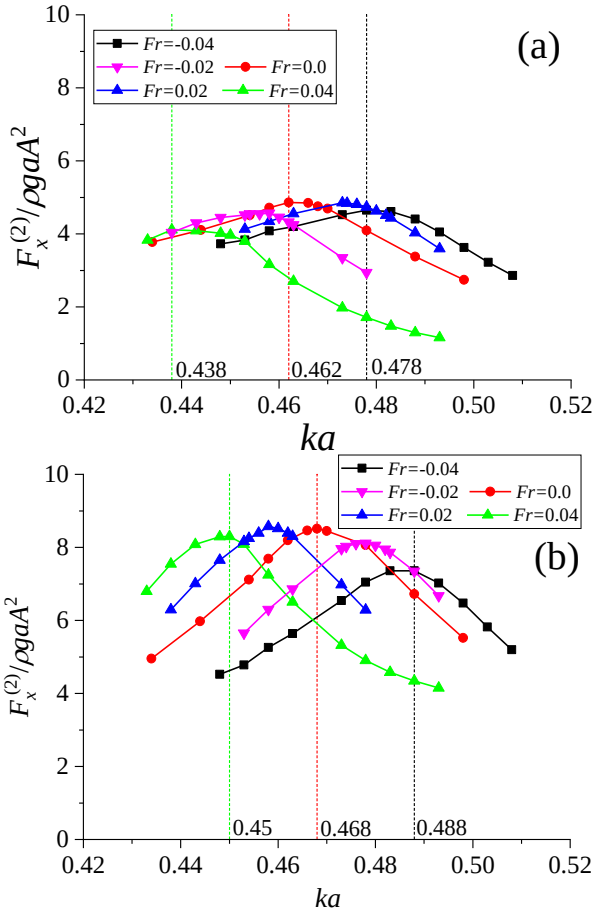

Fig. 24. The amplitude of second-order wave forces versus *ka* under five different *Fr*; (a) cylinder 1; (b) cylinder 3.

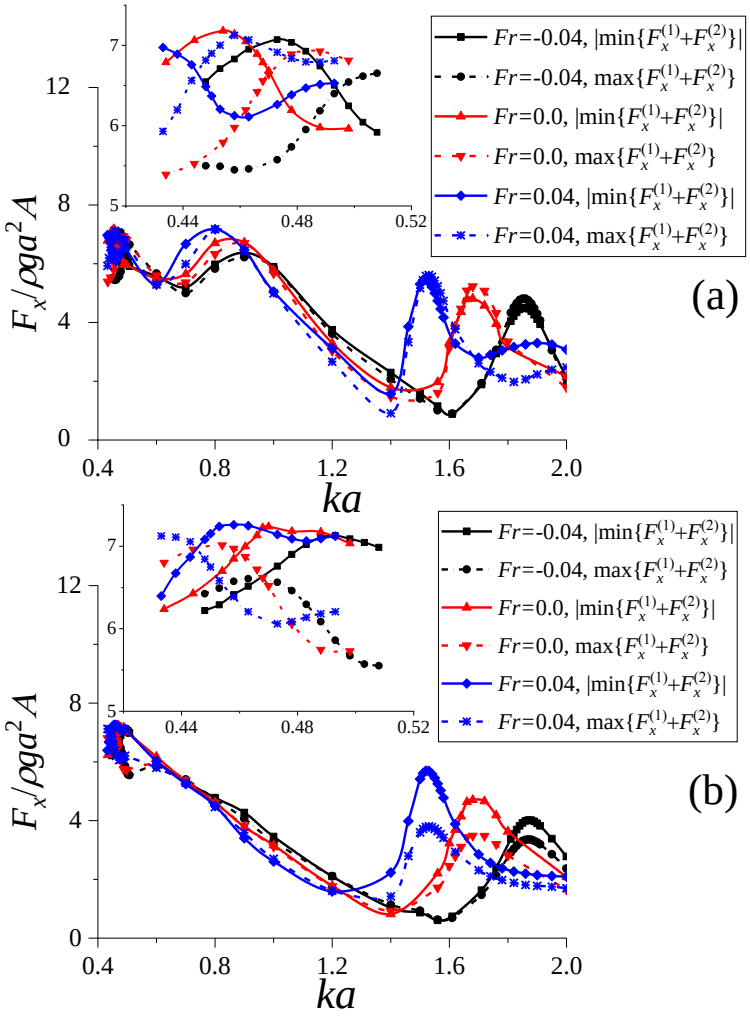

Fig. 25. Peaks and troughs of resultant forces on (a) cylinder 1 and (b) cylinder 3.

The amplitudes of the second-order forces on cylinders 1 and 3 are shown in Fig. 24. The variations trend of second-order force amplitudes with *ka* are quite different from that of second-order wave elevation given in Figs. 13b & 13d and it seems that they do not regularly increase as *Fr* increases. The peaks and troughs of resultant forces at the first-order trapped frequencies increase as *Fr* increases, at the second-order trapped frequencies the peak at cylinder 1 and peak & trough at cylinder 3 also increase as *Fr* increases, which are shown in Fig. 25, in which an enlarged view is also given near the second-order trapped frequencies in each subfigure for the convenience of viewing.

The histories of linear and second-order wave forces on cylinders 1 & 3 in the *x*-direction at first- and second-order near-trapped modes are plotted in Fig. 26. We can see that both linear and second-order forces reach a steady state, and their difference with the development of time at different *Fr* can be clearly observed. The histories of linear and resultant forces on cylinders 1, 2 & 3 in the *x*-direction are shown in Fig. 27, in which the nonlinear feature of forces on cylinders 1 & 3 is relatively evident than that of cylinder 2. In addition, the nonlinear feature of forces at ka=1.88 & Fr=-0.04 is a little different from that at ka=1.52 & Fr=0.04, which indicates that the nonlinear feature of force can be changed by the current

speed.

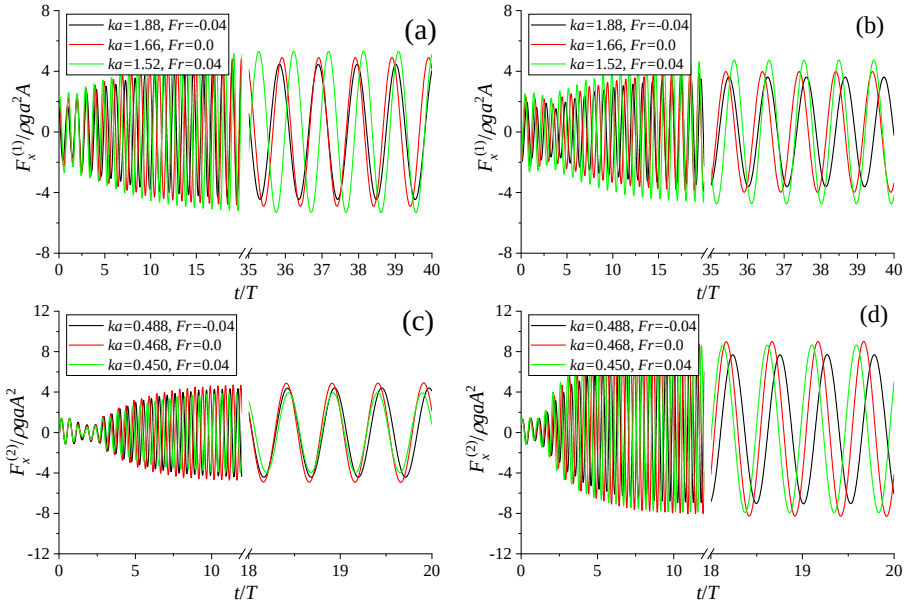

Fig. 26. Histories of forces; (a) first-order force on cylinder 1; (b) first-order force on cylinder 3; (c) second-order force on cylinder 1; (d) second-order force on cylinder 3.

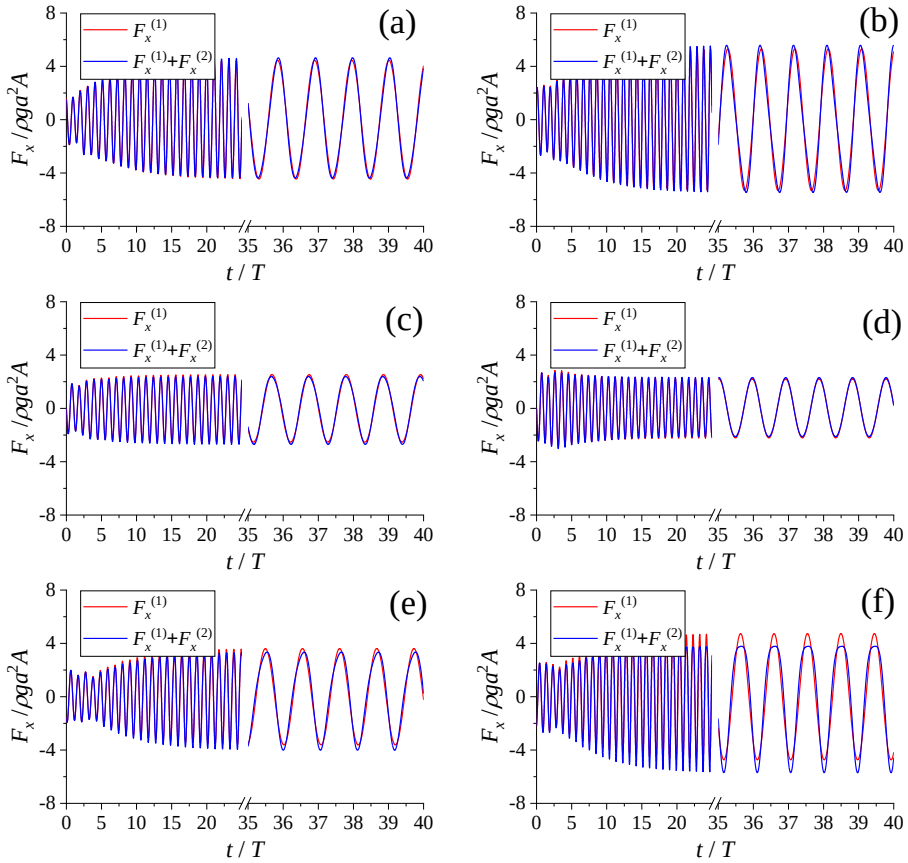

Fig. 27. Histories of forces; (a) & (b) cylinder 1; (c) & (d) cylinder 2; (e) & (f) cylinder 3. (a), (c) & (e): ka=1.88, Fr=-0.04; (b), (d) & (f): ka=1.52, Fr=0.04.

5. Conclusion

Second-order wave diffraction by four cylinders especially for the near-trapping

phenomenon is numerically studied in the present paper. A time-domain FEM with 3-D prismatic elements is used in the simulation. The i-th i=(0, 1, 2) order potentials are obtained by solving the finite element linear system through a combination of CG method and SSOR preconditioner, while the wave elevations and potential on the free surface are updated by the fourth-order Adams-Bashforth scheme.

Validations are made for second-order forces on a single isolated cylinder and linear forces and second-order mean forces on a four-cylinder case to verify the numerical method and good agreement is achieved between the present numerical results and previous studies. The numerical simulations have been made for two four-cylinder configurations, and it is found that the hydrodynamic results of these two cases at different current speed are quite different from those in a single isolated cylinder due to the mutual interference by multiple cylinders.

The numerical result indicate that the near-trapped wave and force are significantly changed by the uniform current. The amplitudes of linear and second-order waves increase as Froude number increases at the near-trapped frequencies, which indicates that the water wave resonance phenomenon is intensified when the current direction is identical to that of the wave propagation (Fr>0). On the contrary, it is weakened when the current propagates oppositely to the direction of wave propagation (Fr<0). Similarity can be found for the linear forces on cylinders. However, the second-order force do not regularly become larger or smaller as Fr increases. The peaks and troughs of the resultant waves and forces at the first-order near trapped mode are generally increasing as the increase of Fr, but the variation is not regular at the second-order near trapped mode.

Acknowledgement

This work was supported by National Natural Science Foundation of China (Grant No. 51679096, 51279179), to which the authors are most grateful.

References

[1]. A.N. Williams and Z. Demirbilek Hydrodynamic interactions in floating cylinder arrays—I. Wave scattering. Ocean Engineering, 1988. **15**(6): p. 549-583.

[2]. A.N. Williams and A.G. Abul-Azm, Hydrodynamic interactions in floating cylinder arrays—II. Wave radiation. Ocean Engineering, 1989. **16**(3): p. 217-263.

[3]. B.P. Butler and G.P. Thomas, The diffraction of water waves by an array of circular cylinders in a channel. Ocean engineering, 1993. **20**(3): p. 295-311.

[4]. A.N. Williams and W. Li, Water wave interaction with an array of bottom-mounted surface-piercing porous cylinders. Ocean Engineering, 2000. **27**(8): p. 841-866.

[5]. D.A.G. Walker and R.E. Taylor, Wave diffraction from linear arrays of cylinders. Ocean Engineering, 2005. **32**(17-18): p. 2053-2078.

[6]. P. Siddorn and R.E. Taylor, Diffraction and independent radiation by an array of floating cylinders. Ocean Engineering, 2008. **35**(13): p. 1289-1303.

[7]. A.G. Abul-Azm and A.N. Williams, Approximation of second-order diffraction loads on arrays of vertical circular cylinders. Journal of fluids and structures, 1989. **3**(1): p. 17-36.

[8]. A.G. Abul-Azm and A.N. Williams, Second-order diffraction loads on arrays of semi-immersed circular cylinders. Journal of Fluids and Structures, 1989. **3**(4): p. 365-387.

[9]. A.N. Williams, A.G. Abul-Azm, and S.A. Ghalayini, A comparison of complete and approximate solutions for second-order diffraction loads on arrays of vertical cirćular cylinders. Ocean Engineering, 1990. **17**(5): p. 427-445.

[10]. S.A. Ghalayini and A.N. Williams, Nonlinear wave forces on vertical cylinder arrays. Journal of fluids and structures, 1991. **5**(1): p. 1-32.

[11]. F. Ursell. Trapping modes in the theory of surface waves. *Mathematical Proceedings of the Cambridge Philosophical Society*. 1951. Cambridge University Press.

[12]. H.D. Maniar and J.N. Newman, Wave diffraction by a long array of cylinders. Journal of fluid mechanics, 1997. **339**: p. 309-330.

[13]. D.V. Evans and R. Porter, Near-trapping of waves by circular arrays of vertical cylinders. Applied Ocean Research, 1997. **19**(2): p. 83-99.

[14]. S. Malenica, R.E. Taylor, and J.B. Huang, Second-order water wave diffraction by an array of vertical cylinders. Journal of Fluid Mechanics, 1999. **390**: p. 349-373.

[15]. C.Z. Wang and G.X. Wu, Time domain analysis of second-order wave diffraction by an array of vertical cylinders. Journal of Fluids and Structures, 2007. **23**(4): p. 605-631.

[16]. J.T. Chen and J.W. Lee, A semi-analytical method for near-trapped mode and fictitious frequencies of multiple scattering by an array of elliptical cylinders in water waves. Physics of Fluids, 2013. **25**(9): p. 097103.

[17]. I.K. Chatjigeorgiou and V. Katsardi, Hydrodynamics and near trapping effects in arrays of multiple elliptical cylinders in waves. Ocean Engineering, 2018. **157**: p. 121-139.

[18]. H. Kagemoto, M. Murai, and T. Fujii, Second-order resonance among an array of two rows of vertical circular cylinders. Applied Ocean Research, 2014. **47**: p. 192-198.

[19]. D. Walker, et al., Wave diffraction and near-trapping by a multi-column gravity-based structure. Ocean Engineering, 2008. **35**(2): p. 201-229.

[20]. J.R. Grice, P.H. Taylor, and R.E. Taylor, Near-trapping effects for multi-column structures in deterministic and random waves. Ocean Engineering, 2013. **58**: p. 60-77.
[21]. W. Bai, et al., Fully nonlinear analysis of near-trapping phenomenon around an array of cylinders. Applied Ocean Research, 2014. **44**: p. 71-81.
[22]. R. Zhao and O.M. Faltinsen, Interaction between waves and current on a two-dimensional body in the free surface. Applied Ocean Research, 1988. **10**(2): p. 87-99.
[23]. J. Nossen, J. Grue, and E. Palm, Wave forces on three-dimensional floating bodies with small forward speed. Journal of Fluid Mechanics, 1991. **227**: p. 135-160.
[24]. J. Grue and D. Biberg, Wave forces on marine structures with small speed in water of restricted depth. Applied Ocean Research, 1993. **15**(3): p. 121-135.
[25]. B. Teng and R.E. Taylor. Application of a higher order BEM in the calculation of wave run-up in a weak current. *The Fourth International Offshore and Polar Engineering Conference*. 1994. International Society of Offshore and Polar Engineers.
[26]. M. Isaacson and K.F. Cheung, Time-domain solution for wave—current interactions with a two-dimensional body. Applied Ocean Research, 1993. **15**(1): p. 39-52.
[27]. K.F. Cheung, M. Isaacson, and J.W. Lee, Wave diffraction around three-dimensional bodies in a current. Journal of Offshore Mechanics and Arctic Engineering, 1996. **118**(4): p. 247-252.
[28]. Z. Liu, et al., Wave-current interactions with three-dimensional floating bodies. Journal of hydrodynamics, 2010. **22**(2): p. 229-241.
[29]. A.C. Feng and W.G. Price, Numerical simulations of the hydrodynamic responses of a body interacting with wave and current over a sloping seabed. Applied Ocean Research, 2018. **79**: p. 184-196.
[30]. A.C. Feng, A.R. Magee, and W.G. Price, Two dimensional wave-current-structure interaction with flat or sloping seabed environment in a linearized framework. Ocean Engineering, 2019. **173**: p. 732-747.
[31]. B. Büchmann, J. Skourup, and K.F. Cheung, Run-up on a structure due to second-order waves and a current in a numerical wave tank. Applied Ocean Research, 1998. **20**(5): p. 297-308.
[32]. J. Skourup, et al., Loads on a 3D body due to second-order waves and a current. Ocean Engineering, 2000. **27**(7): p. 707-727.
[33]. Y.-L. Shao and O.M. Faltinsen. Numerical Study on the Second-Order Radiation/Diffraction of Floating Bodies with/without Forward Speed. *25th International Workshop on Water Waves and Floating Bodies*. 2010.
[34]. Y.L. Shao and O.M. Faltinsen, Second-order diffraction and radiation of a floating body with small forward speed. Journal of Offshore Mechanics and Arctic Engineering, 2013. **135**(1): p. 011301.
[35]. B. Büchmann, P. Ferrant, and J. Skourup, Run-up on a body in waves and current. Fully nonlinear and finite-order calculations. Applied Ocean Research, 2000. **22**(6): p. 349-360.
[36]. M.S. Celebi, Nonlinear transient wave–body interactions in steady uniform currents. Computer methods in applied mechanics and engineering, 2001. **190**(39): p. 5149-5172.

572 [37]. P. Ferrant, Runup on a cylinder due to waves and current: potential flow solution with
573 fully nonlinear boundary conditions. International Journal of Offshore and Polar
574 Engineering, 2001. **11**(01).
575 [38]. W. Koo and M.-H. Kim, Current effects on nonlinear wave-body interactions by a 2D
576 fully nonlinear numerical wave tank. Journal of waterway, port, coastal, and ocean
577 engineering, 2007. **133**(2): p. 136-146.
578 [39]. D.J. Kim and M.H. Kim, Wave-current interaction with a large three-dimensional body
579 by THOBEM. Journal of ship research, 1997. **41**(04): p. 273-285.
580 [40]. F. Hecht, BAMG: bidimensional anisotropic mesh generator. User Guide. INRIA,
581 Rocquencourt, 1998.
582 [41]. T. Chung, Computational fluid dynamics. 2010: Cambridge university press.
583 [42]. Q.W. Ma, G.X. Wu, and R. Eatock Taylor, Finite element simulation of fully non‐
584 linear interaction between vertical cylinders and steep waves. Part 1: methodology and
585 numerical procedure. International Journal for Numerical Methods in Fluids, 2001.
586 **36**(3): p. 265-285.
587 [43]. Q.W. Ma, G.X. Wu, and R. Eatock Taylor, Finite element simulations of fully non‐
588 linear interaction between vertical cylinders and steep waves. Part 2: numerical results
589 and validation. International Journal for Numerical Methods in Fluids, 2001. **36**(3): p.
590 287-308.
591 [44]. H.C. Huang and C.Z. Wang, Finite element simulations of second order wave
592 resonance by motions of two bodies in a uniform current. Ocean Engineering, 2019.
593 **196**: p. 106734
594 [45]. R.E. Taylor and S.M. Huang, Second order diffraction forces on a vertical cylinder in
595 regular waves. Applied Ocean Research, 1987. **9**(1): p. 19-30
596 [46]. C.M. Linton and D.V. Evans, The interaction of waves with arrays of circular
597 cylinders. Journal of fluid mechanics, 1990. **215**: p.549-569